Solid-State Electronics 208 (2023) 108741

Contents lists available at ScienceDirect

Solid State Electronics

journal homepage: www.elsevier.com/locate/sse

GaN hot electron transistors: From ballistic to coherent

J.W. Daulton [a,b], R.J. Molnar [b], J.A. Brinkerhoff [b], Z.C. Adamson [a], M.A. Hollis [b], A. Zaslavsky [a]

[a] School of Engineering, Brown University, Providence, RI 02912, United States
[b] MIT Lincoln Laboratory, Lexington, MA 02421, United States

ARTICLE INFO

The review of this paper was arranged by Prof. Sorin Cristoloveanu

Keywords:
Hot electron transistor
Ballistic transistor
Polarization doping
Atomic layer etching
Coherent transistor

ABSTRACT

Previously we demonstrated high-current, high-gain III-nitride hot electron transistors (HETs) with collimated electron injection into an undoped base region, reaching collector current density of ~0.44 MA/cm^2 and Gummel gain $\beta \sim 2$ at 300 K. Here, we compare the behavior of these devices from 300 to 77 and 4.2 K to elucidate the role of hot electron scattering in limiting the performance. Under cryogenic operation and Gummel biasing, we obtain a maximum current gain of 3.5 at a collector current density of 1.35 MA/cm^2, limited by the onset of intervalley electron transfer, and common-emitter current gain $\beta > 20$. Our results point to the promise of nitride HETs for realizing the long-proposed coherent transistor.

1. Introduction

Gallium arsenide-based hot electron transistors (HETs), where energetic electrons traverse the base ballistically and surmount the base–collector barrier, attracted significant research effort throughout the 1980's [1–3]. However, interest in these devices eventually waned due to the low Γ to L intervalley energy spacing in GaAs, which limited ballistic transport and gain. More recently, progress in III-nitride materials growth, where the large intervalley Γ to M−L energy separation of approximately 2 eV allows for significantly higher injected electron energy before the onset of intervalley scattering, has led several groups to explore nitride-based HETs [4–6], although until recently reported devices were limited to relatively low current densities and gain.

Recently, we reported on room-temperature GaN-based HETs with high common-emitter current gain $\beta = I_C/I_B > 20$ and very high-current operation [7]. In our design, the electron beam was collimated by injecting into the base from a quantized subband formed in the emitter, whereas the base was doped via polarization only, eliminating the ionized impurity scattering that significantly reduced electron mean-free path in most earlier demonstrations. In this work, we extend the room temperature testing to 77 and 4.2 K, demonstrating minimal temperature sensitivity in the *I-V* characteristics and the transfer coefficient $\alpha = I_C/I_E$, as well as a record I_C current density in excess of 1.35 MA/cm^2 at 77 K.

Further, we have observed the onset of intervalley electron transfer [8], as manifested in the Gummel characteristics by the rollover in differential transfer coefficient at high V_{BE}. Our high α and suppressed scattering point to the potential of nitride HETs for experimentally realizing the long-proposed coherent transistor [9,10] that requires fully ballistic transport at cryogenic temperatures.

2. Device design and fabrication

Our device structure is shown schematically in Fig. 1(a) together with a top view of the device with a ~1.3 μm^2 emitter area. Device design simulations in Synopsys Sentaurus were used to ensure formation of a high-density 2D electron gas (2DEG) in the base, with electron injection energy under active biasing not to exceed the Γ to M−L intervalley energy spacing. Such design checks can be reliably performed with Poisson, drift–diffusion, and 1-D Schrödinger solvers. It would be interesting to simulate the full *I-V* characteristics of our device, but this is impeded by the lack of reliable AlN tunneling mass and hot electron scattering time constants, as well as the difficulty of treating hot and cold electron populations simultaneously in the GaN base. The resulting epitaxial design was grown by MOCVD on 2″ sapphire wafers. The emitter stack consisted of a ~10^{19} cm^{-3} doped emitter cap, with a triangular quantum well formed by polarization fields at the interface of an undoped graded AlGaN emitter and an ultrathin 1.5 nm AlN tunnel barrier. The base W_B consisted of a narrow 10 nm undoped GaN layer with a designed 2DEG density of ~3.5×10^{12} cm^{-2} formed due to polarization doping at the emitter–base interface. The collector region consisted of a graded AlGaN base–collector transition layer to an

E-mail addresses: jeffrey_daulton@brown.edu, daulton@ll.mit.edu (J.W. Daulton).

https://doi.org/10.1016/j.sse.2023.108741

Available online 6 August 2023

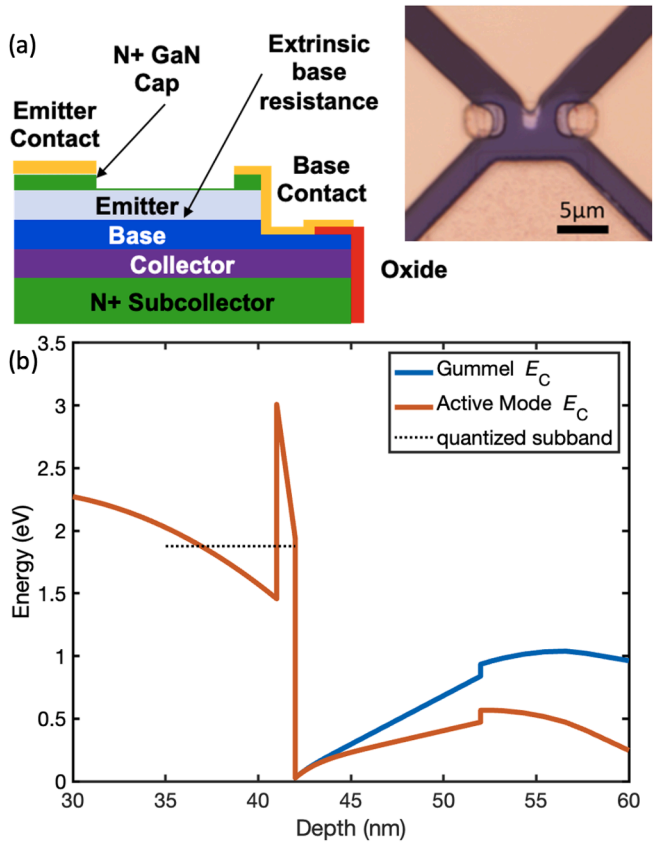

Fig. 1. (a) Schematic cross-section of device (with only one of two symmetric base contacts shown) together with a top-view photograph; (b) self-consistent band diagram for $V_{BE} = 2$ V, $V_{CB} = 0$ (Gummel) and 2 V (active biasing).

$Al_{0.12}Ga_{0.88}N$ collector barrier. The resulting band diagram, including the quantized injection subband in the emitter and the I_C and I_B electron current components, is illustrated in Fig. 1(b). The fabrication details, including damage-free BCl_3/O_2 atomic layer etching to enable low-resistance sidewall contacts to the 2DEG in the base, as well as contact metallization and active-area isolation steps, are available in [7].

3. Electrical characterization

Two HET devices (T1 and T2) were characterized at 300 K and then prepared for low-temperature device testing by wire-bonding to a DIMM PCB configured for immersion in liquid N_2 and He. Fig. 2(a) shows the Gummel plot of device T2 at 300 K up to an I_E current compliance limit of 12 mA, slightly under ~1 MA/cm^2, set to protect the device from emitter metal burnout. Gummel current gain β continues increasing and shows no sign of rollover by the time it reaches a maximum value of 2.5 at $V_{BE} = 4.6$ V. Fig. 2(b) shows the reproducibility of the two devices, with minimal deviation in transfer coefficient α: we observe a slightly higher α in T1 over the entire bias range after onset of hot electron injection. We attribute this slight difference to dislocations within each device, as our measured dislocation density of $\sim 5 \times 10^8$ cm^{-2} [7] results in an average of 5–10 dislocations per emitter, with significant device-to-device variation.

The Gummel condition transfer coefficients of device T2 at 300, 77 and 4.2 K are shown in Fig. 3. At low V_{BE} we observe a delayed onset of hot electron injection at low T, which we attribute to suppressed thermionic filling of the quantized emitter subband. However, once the low-temperature injection commences at $V_{BE} \sim 1.1$ V, there is only a barely noticeable increase in sharpness for 4.2 K compared to 77 K. As the 77 K condition is closest to the peak of sapphire's thermal conductivity, we risked increasing the current compliance to measure the

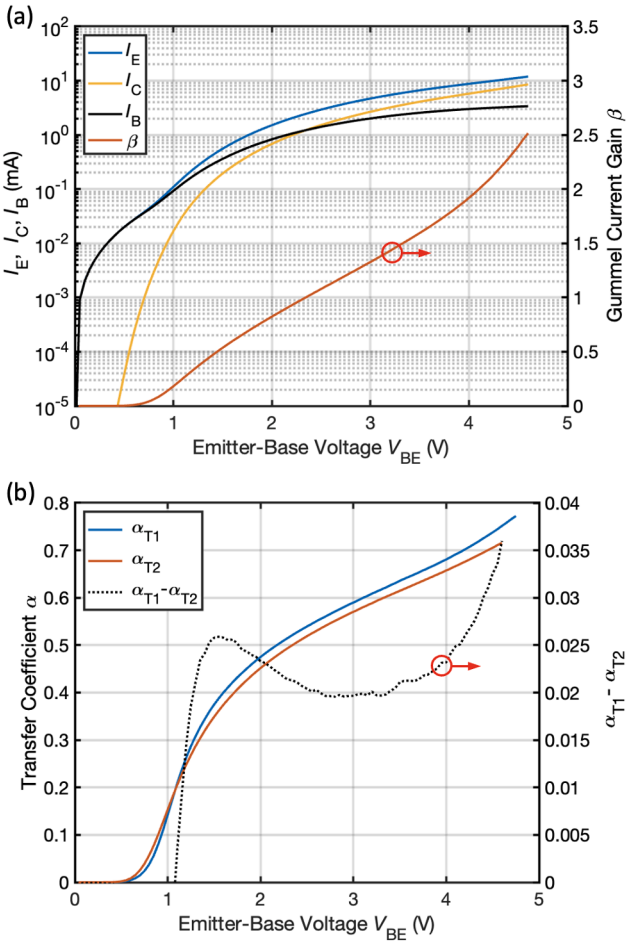

Fig. 2. (a) Room-temperature Gummel ($V_{CB} = 0$) plot of device T2, including all current components and current gain β; (b) transfer coefficient α for devices T1 and T2 and their difference, showing reproducible device behavior.

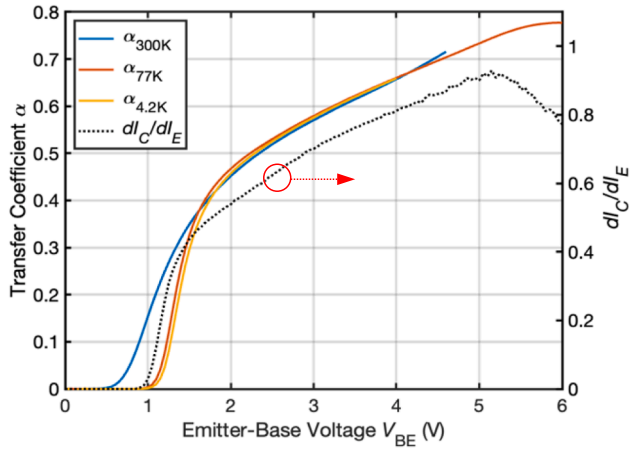

Fig. 3. Transfer ratio α for device T2 at 300, 77 and 4.2 K; differential transfer ratio dI_C/dI_B at 77 K shows onset of intervalley scattering at high V_{BE}.

device up to $V_{BE} = 6$ V, where I_C density reached 1.35 MA/cm^2 and Gummel gain reached 3.5. We also observed a clear rollover in the differential gain dI_C/dI_B at $V_{BE} = 5.1$ V, which we attribute to the onset of intervalley scattering. Measured active mode common-emitter current gain reached $\beta > 20$ for $V_{BE} = 2$ V and $V_{CB} = 2.2$ V active biasing. The

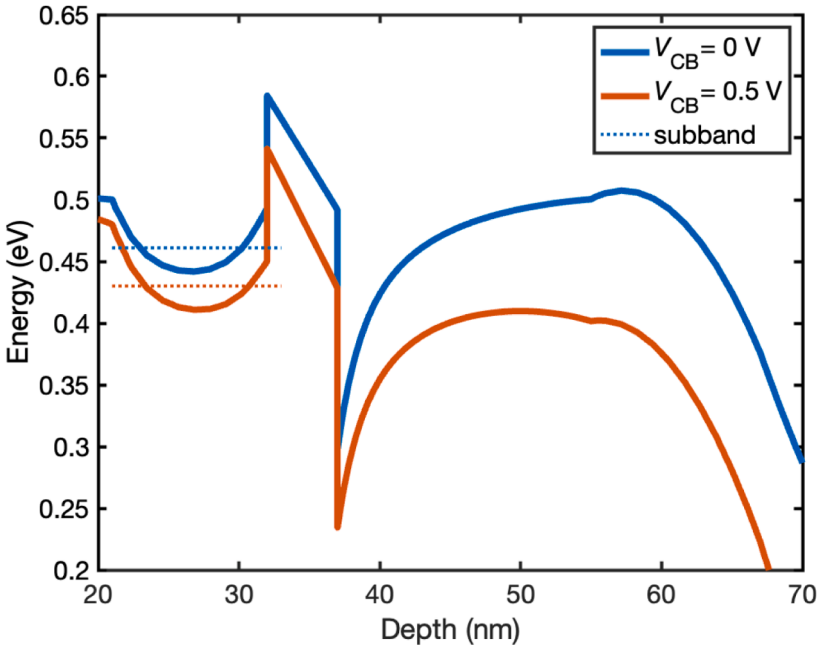

Fig. 4. Preliminary low-energy-injection HET design with modified emitter and tunnel barrier, at $V_{BE} = 0.5$ V, $V_{CB} = 0$ (Gummel) and 0.5 V.

active mode biasing diagram is shown Fig. 1(b), where $V_{CB} > 0$ serves to lower the base–collector barrier and thereby enhance the transfer coefficient α of injected emitter electrons reaching the collector.

The temperature independence of the transfer coefficient at cryogenic temperatures – with α at 77 and 4.2 K being nearly indistinguishable, see Fig. 3 – indicates that the dominant scattering mechanism depends on the electron rather than lattice temperature. This is consistent with LO-phonon emission being the dominant scattering mechanism at low T in the absence of impurity scattering, with $\hbar\omega_{LO} = 92$ meV in GaN [6,11].

4. Towards the coherent transistor

The high measured values of α despite the dominant role of LO-phonon emission indicate that the III-nitride HET is promising for the long-proposed but never realized coherent transistor. Proposed three decades ago by Grinberg and Luryi [9,10], it promises current and power gain at frequencies above the usual f_T cut-off, provided extremely stringent criteria on ballistic transport through the base can be met. A simple physical picture of the coherent transistor operation assumes perfectly monoenergetic electrons traversing the base at the same velocity v_B with no recombination. In the absence of parasitics, a periodic modulation of V_{BE} sets up an electron density wave in the base:

$$n(z,t) = n_0 \exp[i\omega(t - z/v_B)], \tag{1}$$

where n_0 is the amplitude of the injected density modulation. With no scattering, the current density through the base is constant $J(z,t) = -env_B$, leading to a base transport factor $\alpha = \exp[-i\omega\,(W_B/v_B)] = \exp[-i\omega\tau_B]$, where τ_B is the base transit time. This leads to a current gain β [9,10]:

$$\beta = \alpha \Big/ (1-\alpha) = [2|\sin(\omega\tau_B/2)|]^{-1}. \tag{2}$$

For "low" frequencies, $\omega\tau_B < 1$, Eq. (2) reduces to $\beta \sim (\omega\tau_B)^{-1}$, leading to an $f_T = (2\pi\tau_B)^{-1}$, as expected in an HBT limited by the base transit time. However, Eq. (2) also predicts gain peaks at higher ω, set by the condition $\omega\tau_B = 2\pi m$, where m is an integer. Physically, this happens whenever m wavelengths of the electron density wave of Eq. (1) fit into the base W_B, at which point the net injected electron charge is zero and no base current is needed to maintain charge neutrality in the base. The result for this resonant condition is "infinite" gain: output current modulation without any RF base current.

Evidently, the sharp gain peaks predicted by Eq. (2) would be washed out in a real device. Even in the absence of scattering, a spread in the injection velocity v_B due to thermal broadening weakens the resonant gain peaks. Any scattering in the base destroys ballistic transport and adds a normal base current ~ (1–α). Finally, in a real device, the parasitic base resistance as well as the emitter–base and base–collector capacitances would impose additional limitations on f_T due to emitter and collector delays, as in any HBT [12]. Grinberg and Luryi modeled the coherent transistor using an AlGaAs/GaAs HBT and predicted observable gain peaks above f_T by assuming carrier injection into a heavily-doped GaAs base at an energy Δ, with $kT \ll \Delta < \hbar\omega_{LO} \sim 36$ meV. For these conditions, with phonon scattering suppressed and the thermal spread in injection energy minimized by going to $T = 4.2$ K, they predicted impurity scattering in the base to be the main limiting mechanism. The inclusion of parasitics led them to the somewhat counterintuitive result that the coherent transistor above-f_T gain peaks would be easier to observe in devices with a longer base W_B, as long as the base transport remained mostly ballistic [10].

Compared to the AlGaAs/GaAs HBT, the nitride HET has two major advantages. The polarization doping in the base eliminates impurity scattering and the LO-phonon energy is much higher, making this an ideal system for observing coherent transistor gain peaks. But it should be stressed that the injection of electrons at $\Delta < \hbar\omega_{LO} \sim 92$ meV requires a complete redesign of the HET emitter to lower the injection energy compared to Fig. 1(b). A preliminary simulated band diagram under $V_{BE} = 0.5$ V and $V_{CB} = 0$ and 0.5 V is shown in Fig. 4, where the tunnel barrier has been changed to 5 nm of $Al_{0.12}Ga_{0.88}N$, the undoped base thickness W_B increased to 18 nm, and the Al content and doping gradients in the emitter altered to lower the injection energy (here the emitter subband confinement is closer to parabolic than triangular). Additional emitter design flexibility is possible by using InGaN material near the tunnel barrier, at the cost of making the epitaxial growth more complex.

5. Conclusions

We have fabricated a III-nitride HET with temperature-insensitive device characteristics between 77 and 4.2 K, including common-emitter gain > 20 and high ballistic transfer ratio and Gummel gain, at current densities above 1 MA/cm^2 up to the onset of intervalley scattering. This suggests the potential of redesigned nitride HETs for the proposed coherent transistor [9,10], where the electron injection energy is reduced below $\hbar\omega_{LO} \sim 92$ meV above E_F of the 2DEG in the GaN base.

Declaration of Competing Interest

The authors declare the following financial interests/personal relationships which may be considered as potential competing interests: [J. W. Daulton reports financial support was provided by Under Secretary of Defense for Research and Engineering under Air Force Contract No. FA8702-15-D-0001. Co-author A. Zaslavsky is an editor for Solid-State Electronics].

Data availability

Data will be made available on request.

Acknowledgements

Distribution statement A. Approved for public release. Distribution is unlimited. This material is based upon work supported by the Under Secretary of Defense for Research and Engineering under Air Force Contract No. FA8702-15-D-0001. Any opinions, findings, conclusions or recommend-ations expressed in this material are those of the author(s) and do not necessarily reflect the views of the Under Secretary of Defense for Research and Engineering. The lead author acknowledges the support of the Lincoln Scholars Program during his Brown PhD studies. The authors would like to thank G. W. Turner and T. J. Weir for useful discussions.

References

[1] Hollis MA, Palmateer SC, Eastman LF, Dandekar NV, Smith PM. Importance of electron scattering with coupled plasmon-optical phonon modes in GaAs planar-doped barrier transistors. IEEE Electron Dev Lett 1983;4(12):440–3.
[2] Heiblum M, Nathan MI, Thomas D, Knoedler CM. Direct observation of ballistic transport in GaAs. Phys Rev Lett 1985;56:2200–3.
[3] Heiblum M, Anderson I, Knoedler CM. DC performance of ballistic tunneling hot-electron-transistor amplifiers. Appl Phys Lett 1986;49:207–9.
[4] Dasgupta S, Nidhi, Raman A, Speck JS, Mishra UK. Experimental demonstration of III-nitride hot-electron transistor with GaN base. IEEE Electron Dev Lett 2011;32 (9):1212–4.
[5] Yang ZC, Zhang Y, Krishnamoorthy S, Nath DN, Khurgin JB, Rajan S. Current gain in sub-10 nm base GaN tunneling hot electron transistors with AlN emitter barrier. Appl Phys Lett 2015;106. art. 032101.
[6] Gupta G, Ahmadi E, Suntrup III DJ, Mishra UK. Establishment of design space for high current gain in III-N hot electron transistors. Semicond Sci Technol 2018;33. art. 015018.
[7] Daulton JW, Molnar RJ, Brinkerhoff JA, Hollis MA, Zaslavsky A. III-nitride vertical hot electron transistor with polarization doping and collimated injection. Appl Phys Lett 2022;121. art. 223503.
[8] Heiblum M, Calleja E, Anderson IM, Dumke WP, Knoedler CM, Osterling L. Evidence of hot-electron transfer into an upper valley in GaAs. Phys Rev Lett 1986; 56:2854–7.
[9] Grinberg AA, Luryi S. Ballistic versus diffusive base transport in the high-frequency characteristics of bipolar transistors. Appl Phys Lett 1992;60:2770–2.
[10] Grinberg AA, Luryi S. Coherent transistor. IEEE Trans Electron Dev 1993;40: 1512–22.
[11] Jhalani VA, Zhou J-J, Bernardi M. Ultrafast hot carrier dynamics in GaN and its impact on the efficiency droop. Nano Lett 2017;17:5012–9.
[12] Taur Y, Ning TH. Fundamentals of Modern VLSI Devices. 3rd ed. New York: Cambridge University Press; 2022 [chapters 9 and 11].